rGO-BCNT/PANI Three-Dimensional Flexible Aerogel Sponge Electrodes and Electrochemical Performance

Yuhan Wang[#], Siyu Guo[#], Yanzhi Cai[*], Zhongyi Hu, Haiming Yu and Dengpeng Chen

College of Materials Science and Engineering, Xi'an University of Architecture and Technology, Xi'an, Shaanxi 710055, P. R. China

Abstract: Self-supported flexible supercapacitors have promising applications in wearable electronics. The electrode materials, as a crucial component of supercapacitors, have a decisive impact on the energy storage performance of the entire device. Herein, reduced graphene oxide-boron atom doped-carbon nanotubes/polyaniline (rGO-BCNT/PANI) (rBP) three-dimensional (3D) aerogel sponge electrode materials were prepared by a simple ultrasonic self-assembly followed by reduction-induced self-assembly reaction. The rBP aerogel sponge structure not only provided a channel for electrolyte exchange, but also provided enough space for PANI nanoparticles to withstand the volume change during charging and discharging, and inhibited the decomposition of PANI nanoparticles. As a result, the 3D rBP aerogel sponge with 60 mg PANI addition amount (rBP_{60}) exhibited high specific capacitance (695 $F \cdot g^{-1}$), high power density (675 $W \cdot kg^{-1}$), and high energy density (60.95 $Wh \cdot kg^{-1}$) at 0.5 $A \cdot g^{-1}$ in a three-electrode system. The 3D rBP_{60} aerogel sponge electrode material can reach 610 $F \cdot g^{-1}$ at 2 $A \cdot g^{-1}$, with a retention rate of up to 88% after 2000 cycles. The Coulombic efficiency of the rBP_{60} aerogel sponge electrode material was close to or equal to 85.5% at different current densities. The 3D rBP aerogel sponge was exceptionally flexible, maintaining its morphology without damage after 100 compression-release cycles.

Keywords: Reduced graphene oxide, Carbon nanotubes, Polyaniline, Flexible aerogel sponge, Electrochemical properties.

1. INTRODUCTION

Traditional rigid energy storage devices cannot meet the application requirements of flexible electronic devices [1-4]. Therefore, the development of flexible electronic energy storage devices becomes crucial. The remarkable advantages of flexible supercapacitor (FSCs) as an energy storage device, including their exceptional power density, rapid charging and discharging capabilities, and prolonged cycle life, have garnered considerable attention from numerous scientists [5-7]. Electrode is the core component of supercapacitor, so the development of flexible electrode is the key factor to obtain flexible supercapacitor with excellent performance. Conductive polymers are often used as flexible electrode materials [8, 9]. Moreover, based on conductive polymers are typically classified as pseudocapacitors, offering a higher specific capacitance compared to electrochemical double-layer capacitors [10-12]. Among many conductive polymer materials, polyaniline (PANI) has attracted the attention of researchers due to its high theoretical specific capacitance (>1000 F/g), low synthesis cost [13, 14]. However, poor cycling stability and poor mechanical stability limit the use of PANI as an electrode material [15, 16]. It has been shown that the introduction of carbon nanomaterials into polyaniline can solve the above problems [10, 17]. Therefore, the development of compressible flexible hybrid electrode materials is necessary.

Among a variety of carbon nanomaterials, high aspect ratio one-dimensional (1D) carbon nanotubes (CNTs) and high surface area two-dimensional (2D) graphene (GO) have attracted attention [18-21]. Kumar *et al*. [16] synthesized PANI/CNT/GO nanocomposites powder by hydrothermal, and the specific capacitance of the nanocomposites was found to be 312.5 $F \cdot g^{-1}$ at 0.1 $A \cdot g^{-1}$. Due to the powder cannot be independent as electrode, it must be bonded to a flexible substrate for application. However, the bonded powder is extremely prone to flaking and accumulation. Furthermore, the flexible substrate introduces additional mass and does not meet the demand for lightweight materials. 1D CNTs and 2D GO sheets show great potential as electrode materials for FSC due to their excellent mechanical properties [22-24]. Jiang *et al*. [25] designed a PANI/GO/CNT composite film with a specific capacitance of 729.3 $F \cdot g^{-1}$ at 1 $A \cdot g^{-1}$. Cai *et al*. [21] constructed CNT-$PANI_{nw}$/$PANI_{np}$ aerogel buckypaper with the specific capacitance was 1.720 and 1.560 F/cm^2 after 2000 folding in half-unfolding and 200 zigzag folding-unfolding cycles, respectively, with the capacitance retention of 84.0% and 76.2%, at 8 mA/cm^2. Although 2D GO hybrid electrode materials have demonstrated excellent electrochemical and mechanical properties, the aggregation of GO sheet is unavoidable during the preparation and application of electrode materials. Additionally, the amount of active material that can be loaded per unit area of a thin film electrode is limited. Three-dimensional (3D) flexible aerogel sponge electrode is not only compressible and bendable, but also has a larger thickness than thin film flexible electrode, and therefore can load more active materials per unit area [26-30]. Ao *et al*. [31] prepared

[*]Address correspondence to this article at the College of Materials Science and Engineering, Xi'an University of Architecture and Technology, Xi'an, Shaanxi 710055, P. R. China; E-mail: caiyanzhi@xauat.edu.cn

rGO/CNT/Fe_3O_4/PANI electrodes materials by electrophoresis with a specific capacitance of 414.5 $F \cdot g^{-1}$ at 1 $A \cdot g^{-1}$. Hou *et al*. [32] prepared 3D PANI/P-rGO aerogels, the electrodes present good cycling stability. 3D rGO aerogel sponge, as a derivative structure of 2D GO sheets, inherits the inherent properties of GO nanosheets [5, 33]. The stacking of GO sheets within a 3D aerogel sponge is inevitable in theory. Wu *et al*. [34] prepared PANI/rGO composite aerogel electrode materials by introducing PANI as a coating into rGO aerogel structures, which had a specific capacitance of 808 $F \cdot g^{-1}$ at a current density of 53.33 $A \cdot g^{-1}$. Theoretically, introduction of the PANI coating as a splitter, it did not fundamentally change the characteristic of 2D GO sheets that are easy to pile up. Therefore, it is a major challenge to introduce splitter into GO sheets to avoided the stacking properties of GO sheets. As far as our knowledge, there are few literature reports on compressible, flexible aerogel sponge electrode materials constructed from PANI, CNTs and rGO.

Pure CNTs have excellent electrical conductivity, but the low wettability of CNTs limits their use in other applications [35]. Heteroatom modification CNT can not only optimize the conductivity and surface wettability of carbon materials by introducing defects, but also introduce additional pseudocapacitors through reversible Faraday reactions [36-38]. In this paper, the preparation of a 3D aerogel sponge electrode material composed of reduced graphene oxide-boron atom doped-carbon nanotubes/polyaniline (rGO-BCNT/PANI) (rBP) is reported by means of ultrasonic dispersion reduction-induced self-assembly. The successful exfoliation of the GO sheets was achieved using a high-power ultrasonic disperser, and the BCNT was strategically inserted between the GO sheets resembling structural columns within a building. Subsequently, coatings with PANI molecular states attached to the BCNT and GO sheets were formed using chemical reduction. We systematically analyzed the macroscopic microstructure of the rBP aerogel sponge and the electrochemical properties were also systematically investigated. Furthermore, the flexibility of the electrodes was also examined.

2. EXPERIMENT METHODS

2.1. Materials

Boric acid (H_3BO_3), sulfuric acid (H_2SO_4, with 98% purity), potassium permanganate ($KMnO_4$), sodium nitrate ($NaNO_3$), hydrogen peroxide (H_2O_2, with a concentration of 30%), hydrochloric acid (HCl, with a concentration of 5%), polyaniline (PANI), N-methyl-2-pyrrolidone (NMP) and L-ascorbic acid (L-AA) were purchased from Sinopharm Chemical Reagent. Carbon nanotubes (CNTs) and crystalline flake graphite were obtained from Chinese Academy of Sciences Chengdu Organic Chemicals Co., LTD.

2.2. Preparations

2.2.1. Graphene Oxide (GO) Dispersion Liquid

70 mL of 98% H_2SO_4 was completely dissolved in 1 g of $NaNO_3$ at room temperature.

$$NaNO_3 + H_2SO_4 \rightarrow NaHSO_4 + HNO_3$$

$$4HNO_3 \rightarrow 4NO_2 \uparrow + O_2 \uparrow + 3H_2O$$

The solution was cooled to 0–4 , 2g flake graphite was added, stirring for 40 min, 8 g $KMnO_4$ was added and stirring for 30 min.

$$KMnO_4 + 3H_2SO_4 \rightarrow K^+ + MnO_3^+ + H_3O^+ + 3HSO_4^-$$

$$MnO_3^+ + MnO_4^- \rightarrow Mn_2O_7$$

When the solution turned dark green, the temperature was increased to 40 ℃ and stirred for 5 h.

$$Mn_2O_7 \xrightarrow{\Delta} 6MnO_2 + 3O_2 \uparrow + O_3 \uparrow$$

$$2MnO_2 + 2H_2SO_4 \rightarrow 2MnSO_4 + O_2 \uparrow + 2H_2O$$

240 mL deionized water was added, and the temperature was controlled at 65–75 , stirring for 2h. Heating to 95 and stirring for 5 min, and then 25 mL 30% H_2O_2 was added. After stirring for 30 min, 40 mL 5% HCl was added and the reaction was stopped. Then the suspension was washed to neutral and concentrated to 2 mg/mL and set aside.

2.2.2. Preparation of BCNT

To prepare BCNT, CNTs were ground and mixed with boric acid (H_3BO_3) in a mortar at a mass ratio of 1:10, and the mixed powder was dispersed in 120 mL of deionized water and transferred to an autoclave with a volume of 150 mL. Hydrothermal treatment was carried out at 200 °C for 8h, and BCNT powder was obtained after washing and vacuum drying.

2.2.3. rBP Aerogel Sponge

BCNT (20 mg) and GO (10 mL, 2 mg/mL) dispersions were ultrasonicated in a 1:1 mass ratio for 2-4 h to obtain a well-mixed dispersion a. PANI (40, 60, 80, 100 mg) was ultrasonically dispersed in NMP (4, 6, 8, 10 mL) to prepare a dispersion b. Dispersion a and b were ultrasonically mixed for 30 min and then allowed to stand, 80 mg of ascorbic acid was added, and heat-treated for 2 h at 90 °C. ascorbic acid, and heat-treated at 90 °C for 2 h. After freeze-drying, aerogel materials were obtained, and the samples corresponding to different PANI contents were labeled as rBP_{40}, rBP_{60}, rBP_{80}, and rBP_{100} (Figure **1**).

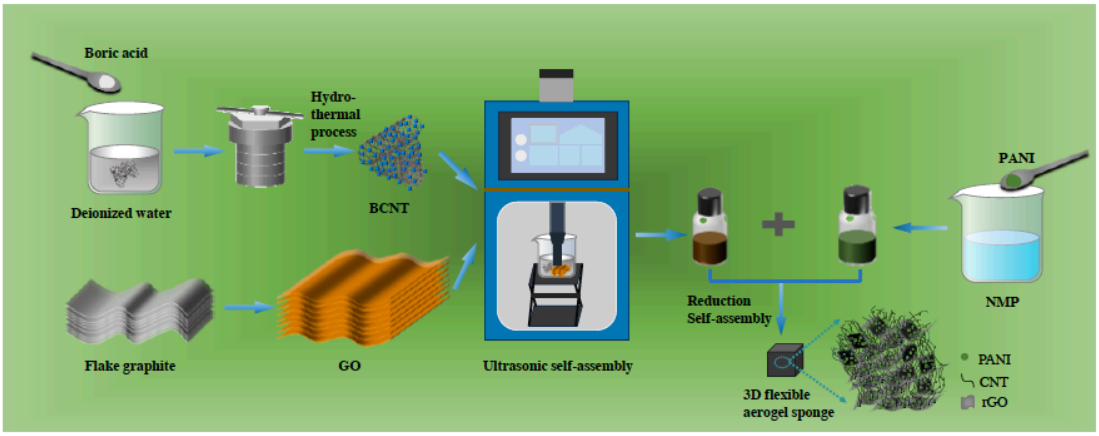

Figure 1: Schematic illustrations for rBP_x by the ultrasonic self-assembly and reduction reaction-based self-assembly method.

2.3. Microstructure Characterization

Field emission scanning electron microscopy/energy dispersive X-ray spectroscopy (FESEM-EDX, Gemini SEM 300) was used to observe the microscopic morphology of rBP_x aerogels. The chemical composition and structure of rBP_x aerogels in the 2θ range of 10 ~ 50° were analyzed by X-ray diffractometer (XRD, Rigaku D/ max-2400, Japan). The rBP_x aerogels were analyzed by Fourier transform infrared (FT-IR) spectroscopy on a Nicolet IS5 infrared spectrometer. And X-ray photoelectron spectroscopy (XPS) was performed using a Thermo SCIENTIFIC ESCALAB Xi+.

2.4. Electrochemical Measurements

2.4.1. Electrochemical Measurements of the rBP Aerogel Sponge Electrodes

The electrochemical tests were performed on an electrochemical workstation (CHI660E, Chenhua, Shanghai, China) using a three-electrode system with 5 M NaOH electrolyte, in which the working electrode was rBP_x aerogel sponge, the reference electrode was Ag/AgCl electrode, and a 1 × 1 cm^2 platinum sheet was used as the counter electrode. Constant current charge/discharge (GCD) and cyclic voltammetry (CV) were measured within a voltage window of -0.3 ~ 0.5 V. The electrochemical impedance spectroscopy (EIS) was carried out to measure the current and cyclic voltammetry (CV). Electrochemical impedance spectroscopy (EIS) measurements were performed over a frequency range of 10^{-2} Hz-10^5 Hz with an alternating current (AC) amplitude of 5 mV.

The specific capacitance of the electrodes is calculated as

$$C_m = (I\Delta t)/(m\Delta V)$$

where C_m ($F\text{-}g^{-1}$) is the mass specific capacitance, m (g) is the electrode mass, Δt (s) is the discharge time, I (A) is the discharge current, and ΔV (V) is the voltage window.

The energy density E (Wh/cm^2) and power density P (W/cm^2) of the rBP_x aerogel sponge electrodes were derived from the following equations.

$$E = \frac{1}{3.6} \times \frac{1}{2} CV^2$$

$$P = \frac{E}{\Delta t} \times 3600$$

where C, ΔV, and ΔT correspond to the specific capacitance ($F \cdot g^{-1}$) of the rBP_x window (V) and the discharge time (s), respectively.

The equation for the Coulomb efficiency of the rBP_x aerogel sponge electrode is calculated from the GCD curve as follows.

$$\eta = \frac{C_c}{C_d}$$

C_c is the capacity calculated according to the discharge time of GCD curve, and C_d is the capacity calculated according to the charge time of GCD curve, and the unit is F/g.

3. RESULTS AND DISCUSSION

3.1. Macro/microstructure Characterization

The aerogel material prepared by the self-assembly process can recover to its original state after compression to 50% thickness, showing excellent flexibility and resilience (Figure **2a**). The 3D rBP aerogel sponge was exceptionally flexible, maintaining its morphology without damaged after 100 compression-release cycles. Therefore, the 3D flexible rBP aerogel sponge had the potential to be a new wearable flexible energy storage material. Figure **2b** was the SEM photo of CNTs inserted between the separated GO nanosheets after ultrasonic

self-assembly. The GO nanosheets were stripped by ultrasonic cavitation and CNTs were dispersed simultaneously. When the sound pressure reached a certain value, the cavitation bubble expands rapidly and explodes in a very short time, producing local high temperature and high pressure. Strong shock waves and high-speed jets separated the graphene oxide nanosheets from each other, speeding up the mass and heat transfer processes, and thus evenly dispersing the CNTs. The dispersed CNTs were randomly inserted between the separated GO nanosheets to prevent them from agglomerating, forming a 3D porous network skeleton of rGO nanosheets being separated and supported by CNTs in Figure **1**. Therefore, the 3D flexible rGO-CNT/PANI flexible aerogel sponge was very lightweight and could be held up by a leaf, as shown in Figure **2c**. Due to the strong interaction between the π bond surface of CNTs/rGO and the conjugated structure of PANI, the graphite structure of CNTs/rGO was strongly bound to the aromatic ring of PANI [21]. Moreover, CNTs have excellent elastic deformation capacity. Therefore, the 3D porous network skeleton is very flexible and robust.

Figure **3** showed the microscopic morphology of the aerogel after freeze-drying. As shown in Figure **3**(**a**), the large number of folds presented on the sample surface indicated the formation of a three-dimensional interconnected aerogel network structure, in addition to the observation of a large number of BCNTs distributed in the muslin-like rGO, which were interspersed between the muslin-like rGO nanosheets, effectively inhibiting the agglomeration of the rGO nanosheets and strengthening the connection between the rGO nanosheets, so that the formation of a three-dimensional network structure more stable. Figure **3**(**b**) showed a structure indicating that PANI nanoparticles can fill in the pores of the 3D network structure composed of BCNTs and rGO. In the whole structure, the rGO aerogel prepared by reduction-induced self-assembly reaction acted as the 3D network substrate, the BCNTs acted as bridges connecting between the rGO nanosheets to reinforce the 3D structure, and the PANI fills in to provide the pseudocapacitance, forming a special structure that can not only significantly inhibit the agglomeration of the nanosheets by utilizing the introduced BCNTs and PANI nanoparticles, but also enable the PANI nanoparticles to have enough space to withstand the charge-discharge process. Particles had enough space to withstand the volume change during the charging and discharging process, effectively inhibiting the powdery decomposition of PANI (Figure **3c**). In addition, C and N elements were also observed to be uniformly dispersed in the samples (Figure **3e** and **f**).

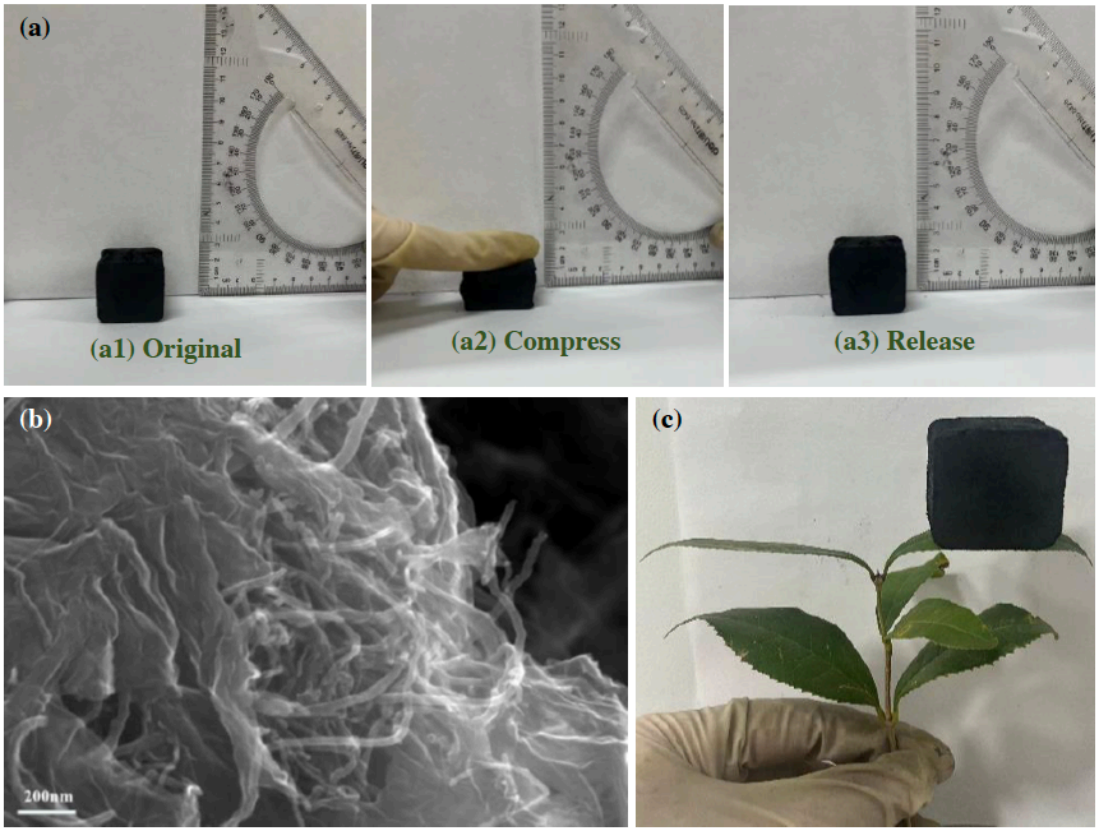

Figure 2: (**a**) The compression-release process of the 3D aerogel sponge: (a1) the original sample; (a2) compress to 50% of the original thickness and (a3) elastic recovery after pressure release; (**b**) SEM photograph of BCNT/GO precursor after ultrasonic self-assembly and (**c**) the 3D aerogel sponge is held up by a leaf.

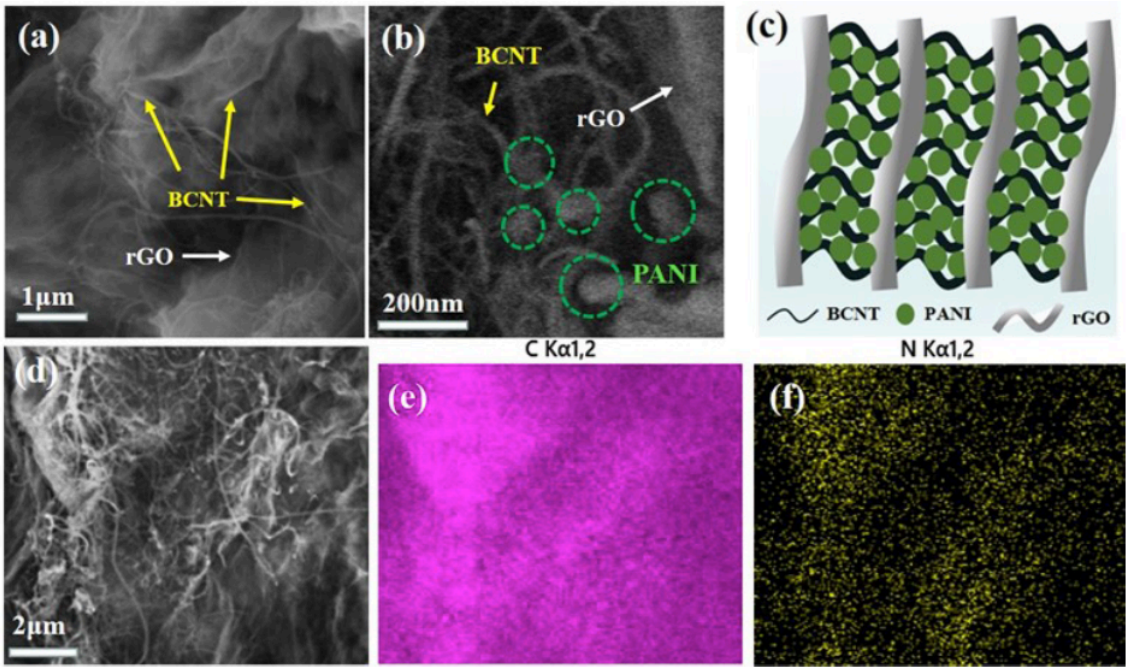

Figure 3: rBP_x composite aerogel sponge: (**a**) and (**b**) distribution of BCNT, rGO and PANI; (**c**) 3D aerogel sponge cross-section structure schematics; (**d**) SEM photo; (**e**) and (**f**) surface scanning EDX analysis of elements C and N in (**d**).

Figure **4**(**a**) showed the IR spectra of rBP_x aerogels sponge with different contents of PANI nanoparticles. The IR spectral lines of rBP_x aerogels had similar shapes, and the positions and numbers of characteristic peaks were the same. All the curves showed characteristic peaks at 1296 cm^{-1}, 1590 and 1496 cm^{-1}, 1147 and 820 cm^{-1}, and 3300-3500 cm^{-1}. Among them, the characteristic peak observed at 1296 cm^{-1} is attributed to C-N stretching vibrations, those at 1590 and 1496 cm^{-1} were related to C=C stretching vibrations of the quinone and benzene rings, respectively, those at 1147 and 820 cm^{-1} reflect in-plane and out-of-plane bending of the C-H bond, and those at 3300-3600 cm^{-1} were attributed to N-H stretching vibrations [39, 40]. The crystal structures of rBP_x aerogel sponge and PANI with different contents of PANI nanoparticles were characterized using XRD. Figure **4**(**b**) showed the XRD spectra of rBP_x aerogel sponge and PANI. PANI had a broad peak centered at θ = 20°, which originates from the orientation of the polyaniline molecular chains, indicating that the polyaniline chains were ordered in the short-range and disordered in the long-range, and the characteristic peak at 25.1° corresponds to (110) crystal surface [41]. All rBP_x aerogel sponge curves had similar shapes and roughly the same peak locations, which suggested that the aerogels with different PANI contents share the same structure. The broad peaks at 21.3° and 43.1° were due to the reflection of the (002) and (100) crystallographic planes after the chemical reduction of GO to rGO, and also the broad peaks indicated the poor crystallinity within the aerogel, which was due to the fact that PANI and BCNTs greatly inhibit the agglomeration of rGO nanosheets. The characteristic peak appearing at 25.1° in polyaniline, the position of the peak was shifted in the rBP_x aerogel sponge, and the diffraction peak became wider and smaller, which proved that the orientation of the introduced PANI molecular chain was disrupted, the crystallinity became worse, and PANI was randomly populated in the three-dimensional aerogel structure, which can be corroborated with SEM. The Raman spectra of rBP_x and rGO aerogels sponge were shown in Figure **4**(**c**)-(**d**), which showed obvious characteristic peaks at 1350 cm^{-1} and 1580 cm^{-1}, corresponding to the D and G peaks of the materials, respectively. The D peak originated from the telescopic vibration of the C-C bond and the C=C double bond, which was a typical Raman peak in CNTs and rGO, and the intensity and the shape of the D peak can reflect the structure of the sample and the defects. The G peak mainly came from the telescopic vibration of sp^2 hybridized carbon atoms and π-electrons in the material, and the intensity of the G peak reflected the number of layers and the integrity of the lattice of the material [42].

In addition, the intensity ratio of D and G bands (I_D/I_G) was used to measure the degree of ordering. For rGO aerogels, the intensity of I_D/I_G can reach 1.10, suggesting that structural defects induced by reduction reaction-induced self-assembly and random distribution of small graphene sheet aggregates increased the degree of disorder. The I_D/I_G intensities of rBP_x aerogels sponge are basically the same ($I_D/I_G \approx 1$), but both were smaller than that of rGO, which suggested that the agglomeration of graphene sheets during reduction was greatly reduced due to the connection of BCNT between rGO nanosheets. In

addition, the three-dimensional network substrate formed by BCNT and rGO will provide space for the presence of PANI nanoparticles. Thus BCNT, rGO and PANI synergized with each other to form a highly ordered 3D aerogel structure. Figure **4**(**e**) showed the X-ray photoelectron spectroscopy (XPS) of rBP_x aerogel sponge, using XPS the electronic states of the elements can be investigated [43, 44], from the XPS spectrum the elements present in the rBP_x aerogel sponge and their contents can be derived, *i.e*., the C (284.8 eV, 78.26%), the N (400.01 eV, 17.56%), and the B (192.88 eV, 4.17%) elements. Five different electronic states were shown in the high-resolution XPS of the C1s region, located at 284.8, 285.5, 286.2, and 288.5 eV, which were assigned to sp^2 C−C, sp^3 C−C, C−N and C=O bonds, respectively (Figure **4f**). The B1s spectrum was deconvoluted into three peaks with the binding energies equal to 191.0, 192.3, and 193.0 eV (Figure **4g**). These peaks were attributed to the B atoms in clusters in BC_3, BC_2O and BCO_2 molecules, respectively [45].

3.2. Electrochemical Performance of rBP Aerogel Sponge Electrodes

The electrochemical performance of rBP_x aerogel sponge electrodes was tested in a three-electrode system containing 5 M NaOH electrolyte, and the

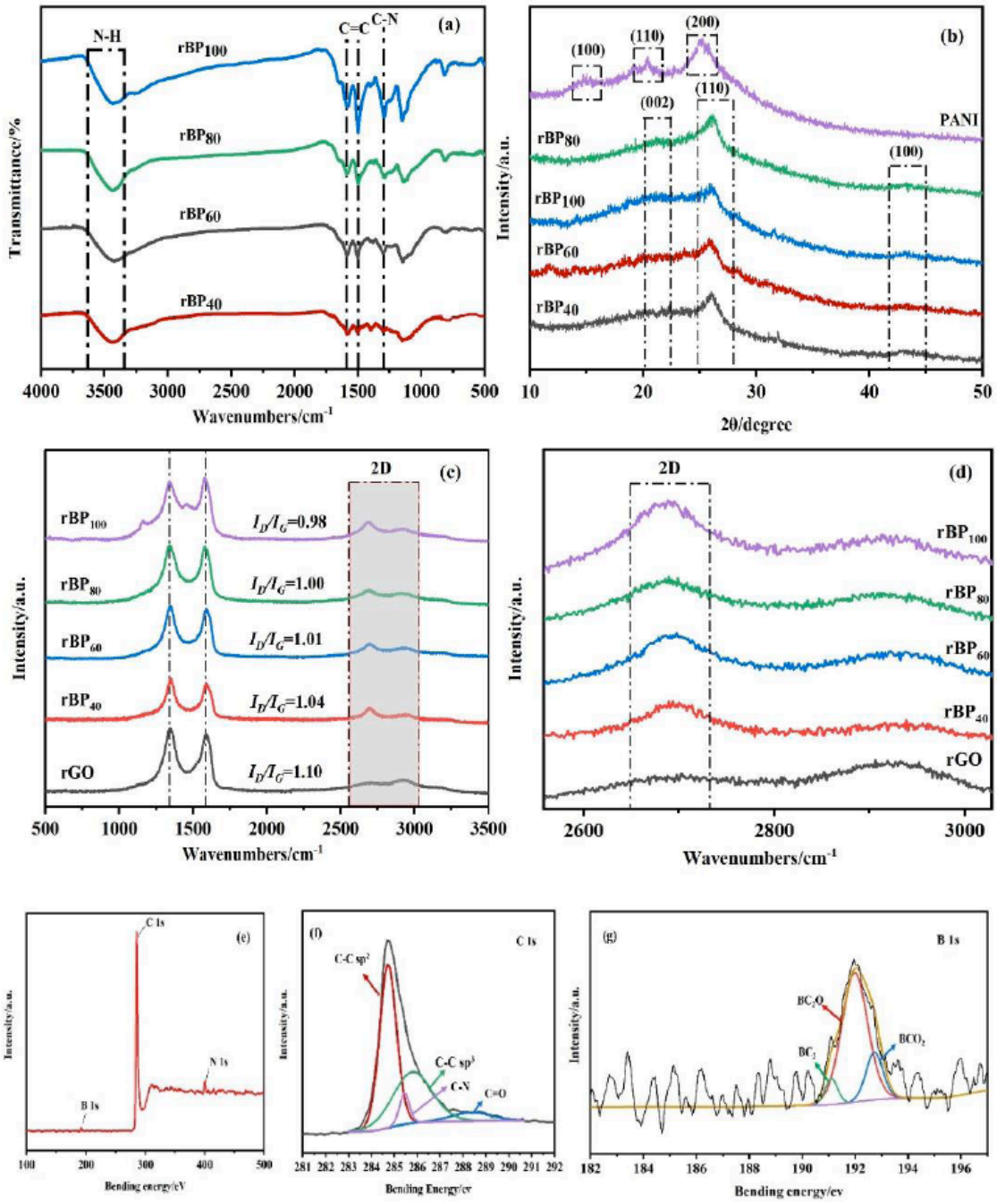

Figure 4: rBP_x aerogel sponge: (**a**) Infrared spectrogram (**b**) XRD spectrum [46] (**c**)-(**d**) Raman spectra (**e**) Full XPS spectrum (**f**) C1s (**g**) B1s.

aerogel electrodes were evaluated by CV, GCD, and EIS, as shown in Figure **5**. Figure **5**(**a**) showed the CV curves of the rBP_x aerogel sponge at a scan rate of 7 mV/s. rBP_{40}, rBP_{60}, rBP_{80}, and rBP_{100} all exhibited obvious redox peaks at a potential of 0.4 V, which corresponded to the typical pseudocapacitive behavior of PANI, and these reversible and successive redox reactions achieved high charge storage capacity and enhance the electrode material's electrochemical performance. With the change of PANI content, the intensity of the redox peaks changed, in which rBP_{40} had the lowest intensity of the redox peaks and rBP_{60} had the highest intensity of the redox peaks. It is worth noting that the intensity of the redox peaks of rBP_x sponge did not increase with the increase of the PANI content, but showed a tendency to increase firstly and then decrease, which should be related to the structure of the aerogel. In addition, as shown in Figure **5**(**a**), the CV curve of rBP_{60} had the largest wrapping area, indicating the highest specific capacitance. The GCD curves of rBP_x aerogels sponge were shown in Figure **5**(**b**). The GCD curves of rBP_x aerogels sponge with different PANI contents all showed a weak plateau around the potential of 0.1-0.2 V, which corresponded to the potential of the redox peaks in the CV curves, and furthermore, the GCD curves were all roughly symmetric at a current density of 1.5 A/g. The mass specific capacitances values of the rBP_{40}, rBP_{60}, rBP_{80} and rBP_{100} aerogels sponge were 372.86 F/g, 621.71 F/g, 409.29 F/g, and 327.86 F/g, respectively. The high specific capacitance of the electrodes was due to the excellent microstructure of the electrodes, where individual graphene oxide nanosheets were self-assembled into a three-dimensional graphene network using a mild chemical reduction process, and BCNT was used to reinforce the three-dimensional structure and further form a conductive network, which results in the rGO-BCNT three-dimensional network substrate with abundant pores and good mechanical properties to accommodate more electroactive fillers, and absorbed-released the stress generated by PANI during repeated charging and discharging cycles as much as possible. This enabled the rGO-BCNT 3D network substrate to have rich pores and good mechanical properties to accommodate more electroactive fillers and to absorb-release the stress generated by the PANI during repeated charge/discharge cycles as much as possible to minimize the damage to the PANI. Even if some of the PANI decomposed during the charge/discharge cycles, the pulverized particles were still confined in the rGO-BCNT 3D network substrate, which effectively inhibited the further decomposition and shedding of the PANI. The Nyquist curve of the rBP_x aerogel sponge and a magnified view of the high-frequency region were given in Figure **5**(**c**).

In general, the intercept on the real axis in the high-frequency region denoted the equivalent series

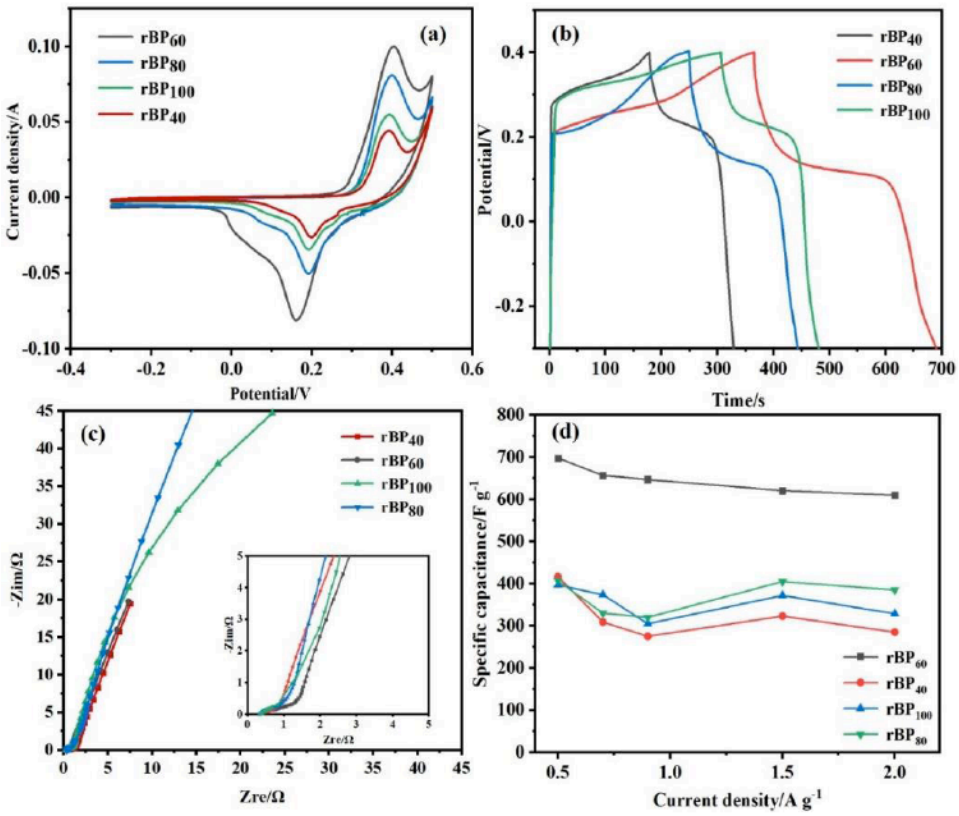

Figure 5: Electrochemical performance of rBP_x aerogel sponge electrode: (**a**) CV curve at a scan rate of 7 mV/s (**b**) GCD curve at a current density of 1.5 A/g (**c**) Nyquist curve and zoomed in high frequency region.

resistance (R_s), which included the resistance of the electrolyte and the electrode sheet as well as the contact resistance between the solid/liquid interface. In the high-frequency region, the small semicircle indicated the fast charge transfer resistance (R_{ct}) at the electrode/electrolyte interface as well as the fast kinetics. All curves were observed as a distinct small semicircle in the high-frequency region and a straight line almost perpendicular to the horizontal axis in the low-frequency region, which indicated that the electrode has a good charge transfer behavior and typical capacitive properties. The R_{ct} and R_s of the aerogels sponge with different PANI contents can be clearly seen in the enlarged graphs in the high frequency region. It was found that the R_s of all four PANI contents of the aerogels were less than 1 Ω, and the R_{ct} was less than 3 Ω, with rBP_{60} obtaining the smallest R_{ct} and R_s, which suggested that the rBP_{60} can provide a better capacitive behavior. In addition, we compared the average specific capacitance of the aerogel electrodes with different PANI contents when the current density was increased from 0.5A/g to 2.0A/g, as shown in Figure **5d**. rBP_{60} showed A specific capacitance up to 695F/g at a current density of 0.5A/g, which was significantly higher than other PANI content aerogel electrodes (rBP_{40}:417F/g, rBP_{80}:407F/g, rBP_{100}:397F/g). At the same time, when the current density was increased to 2A/g, the specific capacitance of rBP_{60} can still be maintained at 610F/g, and the capacitance retention rate can reach 87.4%, which was much higher than other aerogel electrodes.

The electrochemical properties of rBP_{60} aerogel sponge were further tested. Figure **6**(**a**) showed the summarized cyclic voltammograms at different scan rates, characterizing the capacitive behavior of rBP_{60} aerogel sponge from 3 mV/s-20 mV/s. It was found that the area surrounded by the curves gradually increased with the increase of scan rate, and when the scan rate was increased from 3 mV/s to 20 mV/s, the curve profiles remained basically unchanged, both of which exhibited a pair of obvious redox peaks, and the redox peaks were only slightly shifted, which indicated that the rBP_{60} aerogel sponge still had a stable structure at large scan rate. Figure **6**(**b**) showed a summary plot of constant-current charging and discharging at different current densities, and the charging and discharging performance of rBP_{60} aerogel sponge was tested from 0.5 A/g-2.0 A/g. The test results showed that due to the introduction of the PANI pseudocapacitance, the GCD curve did not show a completely symmetrical isosceles triangle shape, but a weak plateau appeared around 0.1 V-0.2 V and corresponded to the potential of the redox peak in the CV curve. The C_S values of rBP_{60} aerogel sponge at densities of 0.5, 0.7, 0.9, 1.5, and 2.0 A/g were 695, 657, 647.86, 621.71, and 610.29 F/g, respectively. rBP_{60} aerogel sponge had a retention of

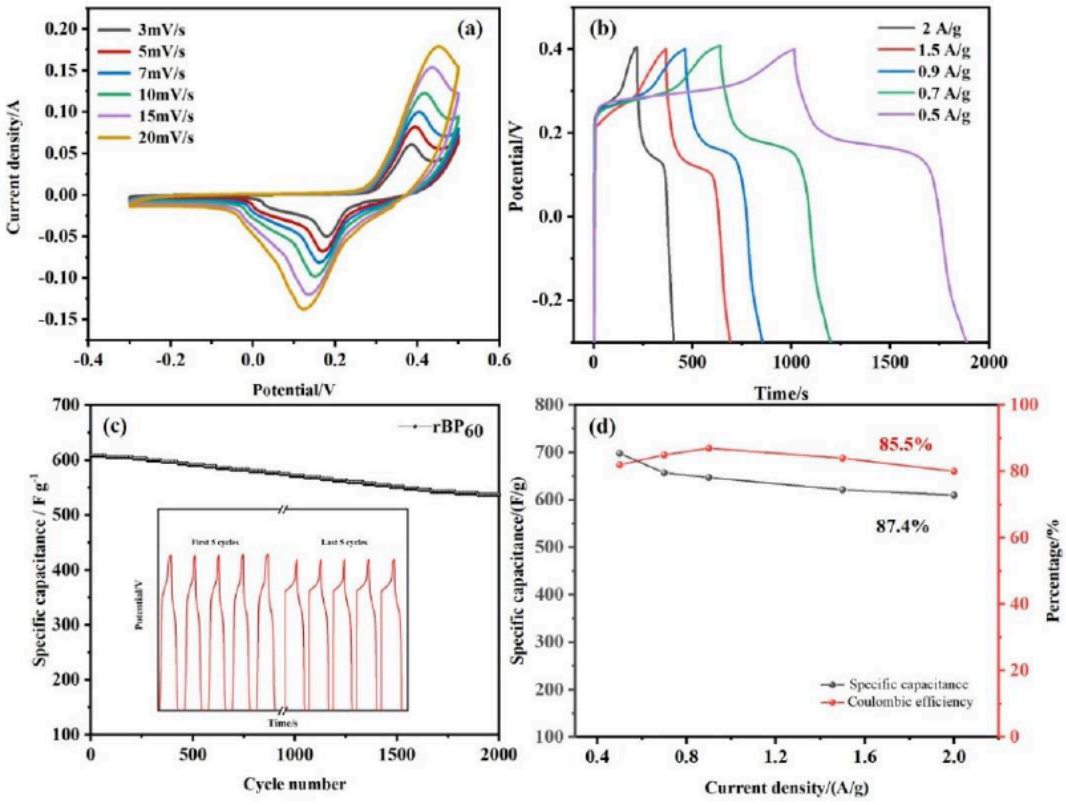

Figure 6: Electrochemical performance of rBP_{60} aerogel sponge electrode: (**a**) GCD curves for different current densities; (**b**) CV curves for different scan rates; (**c**) Capacitance retention after 2000 cycles at constant current density of 2A/g; (**d**) Specific capacitance and coulombic efficiency of rBP_{60} in different current density.

Table 1: Electrochemical Performance of PANI/rGO Electrodes

Electrode	Cs (F/g)	Cycling Stability	Flexible Electrode	Ref.
PANI/rGO powder	432 at 1 A/g	85% @10 000 at 1 A/g	Not reported	[47]
F-rGO/PANI powder	459 at 0.5 A/g	80% @2000 at 7 mA/cm^2	Not reported	[48]
PANI/rGO powder	102 at 1 A/g	85% @1000 at 1 A/g	Not reported	[49]
PANI Fs/FrGO powder	324.4 at 1 A/g	83.3% @1000 at 10 A/g	Not reported	[50]
GNP/PANI/MoS_2 powder	236.23 at 0.5 A/g	91.87%@1000 at 0.5A/g	Not reported	[51]
PANI/PVA/AMTP/CNTs powder	389.5 at 0.5 A/g	83.87%@10000 at 0.5A/g	Not reported	[52]
CNT@PANI@s-GN powder	419 at 5mV/s	Not reported	Not reported	[53]
CMC-PANI/CNT film	348.8 at 0.5 A/g	89.2%@5000 at 0.5A/g	Not reported	[54]
rGO-BCNT/PANI 3D aerogel sponge	695.7 at 0.5 A/g	88%@2000 at 2 A/g	compression-release 100 cycles	This work

87.4% of C_S when the current density was increased from 0.5 to 2.0 A/g, indicating that rBP_{60} aerogel sponge has a higher multiplicity capacity. Cyclic stability of rBP_{60} aerogel sponge was tested at 2 A/g for 2000 cycles (Figure 6c). The cycle test show that the electrode capacitance retention rate could reach 88%, showing a high cycle stability. Meanwhile, the Coulombic efficiency of the rBP_{60} aerogel sponge electrode was close to or equal to 85.5% at different current densities (Figure **6d**). The high multiplicity performance and Coulombic efficiency indicated that the material was expected to realize fast charging in the future, and the highest energy density of 60.95 W h kg^{-1} was achieved at a power density of 675 W kg^{-1}. In summary, BCNT, rGO and PANI were assembled into a system by self-assembly method. rGO and BCNT not only established a porous 3D network, but also made PANI nanoparticles firmly fixed in the system. rBP_x aerogel sponge exhibits higher specific capacitance, better compression-recoil properties than the same material, and its capacitance retention rate after 2000 charge-discharge cycles is close to that of other works (Table **1**). Herein the 3D porous structure of rBP_x aerogel sponge electrode constructed in this work had excellent electrochemical properties and flexibility.

4. CONCLUSION

In this work, the 3D rBP aerogel sponge electrodes were prepared by a simple ultrasonic self-assembly followed by reduction-induced self-assembly reaction. The C_S values of the rBP_{60} aerogel sponge at current densities of 0.5, 0.7, 0.9, 1.5 and 2.0 $A{\cdot}g^{-1}$ were 695, 657, 647.86, 621.71, and 610 F/g, respectively. When the current density was increased from 0.5 $A{\cdot}g^{-1}$ to 2.0 $A{\cdot}g^{-1}$, the Cs retention rate reached 87.4%, indicating that the rBP_{60} aerogel sponge had excellent rate performance. The Cs of the rBP_{60} aerogel sponge was 685 $F{\cdot}g^{-1}$ at 2.0 $A{\cdot}g^{-1}$, and it exhibited an impressive retention rate of 88% after 2000 cycles, thus demonstrating exceptional electrochemical stability. The 3D rBP60 aerogel sponge showed excellent electrochemical properties, which is attributed to the synergistic action of rGO, BCNT and PANI. The 3D rBP aerogel sponge exhibited exceptional flexibility, maintaining its morphology intact without damage even after undergoing 100 cycles of compression and release.

REFERENCE

[1] J. Yan, S.H. Li, B.B. Lan, Y.C. Wu, P.S. Lee, Rational Design of Nanostructured Electrode Materials toward Multifunctional Supercapacitors, Advanced Functional Materials 30 (2020). https://doi.org/10.1002/adfm.201902564

[2] J. Huang, Y.P. Xie, Y. You, J.L. Yuan, Q.Q. Xu, H.B. Xie, Y.W. Chen, Rational Design of Electrode Materials for Advanced Supercapacitors: From Lab Research to Commercialization, Advanced Functional Materials 33 (2023). https://doi.org/10.1002/adfm.202213095

[3] X.L. Chen, R. Paul, L.M. Dai, Carbon-based supercapacitors for efficient energy storage, National Science Review 2017; 4: 453-489. https://doi.org/10.1093/nsr/nwx009

[4] Z.F. Zhao, X.J. Wang, M.J. Yao, L.L. Liu, Z.Q. Niu, J. Chen, Activated carbon felts with exfoliated graphene nanosheets for flexible all-solid-state supercapacitors, Chinese Chemical Letters 2019; 30: 915-918. https://doi.org/10.1016/j.cclet.2019.03.003

[5] Y.L. Shao, M.F. El-Kady, L.J. Wang, Q.H. Zhang, Y.G. Li, H.Z. Wang, M.F. Mousavi, R.B. Kaner, Graphene-based materials for flexible supercapacitors, Chemical Society Reviews 2015; 44: 3639-3665. https://doi.org/10.1039/C4CS00316K

[6] L.B. Dong, C.J. Xu, Y. Li, Z.Z. Pan, G.M. Liang, E.L. Zhou, F.Y. Kang, Q.H. Yang, Breathable and Wearable Energy Storage Based on Highly Flexible Paper Electrodes, Advanced Materials 2016; 28: 9313-9319. https://doi.org/10.1002/adma.201602541

[7] T. Lv, M.X. Liu, D.Z. Zhu, L.H. Gan, T. Chen, Nanocarbon-Based Materials for Flexible All-Solid-State Supercapacitors, Advanced Materials 30 (2018). https://doi.org/10.1002/adma.201705489

[8] Y.Q. Han, L.M. Dai, Conducting Polymers for Flexible Supercapacitors, Macromolecular Chemistry and Physics 220 (2019). https://doi.org/10.1002/macp.201800355

[9] Q.Q. Qin, X.D. Du, C.X. Xu, S.G. Huang, W.J. Wang, Y. Zhang, J. Yan, J.Q. Liu, Y.C. Wu, Flexible Supercapacitors Based on Solid Ion Conducting Polymer with High Mechanical Strength, Journal of the Electrochemical Society 2017; 164: A1952-A1957. https://doi.org/10.1149/2.0771709jes

[10] A. Eftekhari, L. Li, Y. Yang, Polyaniline supercapacitors, Journal of Power Sources 2017; 347: 86-107. https://doi.org/10.1016/j.jpowsour.2017.02.054

[11] Y.H. Wang, X. Chu, Z.H. Zhu, D. Xiong, H.T. Zhang, W.Q. Yang, Dynamically evolving 2D supramolecular polyaniline nanosheets for long-stability flexible supercapacitors, Chemical Engineering Journal 423 (2021). https://doi.org/10.1016/j.cej.2021.130203

[12] X. Cao, H.Y. Zeng, S. Xu, J. Yuan, J. Han, G.F. Xiao, Facile fabrication of the polyaniline/layered double hydroxide nanosheet composite for supercapacitors, Applied Clay Science 2019; 168: 175-183. https://doi.org/10.1016/j.clay.2018.11.011

[13] Reddy, P. C. H.; Amalraj, J; Ranganatha, S; Patil, S.S.; Chandrasekaran, S. A review on effect of conducting polymers on carbon-based electrode materials for electrochemical supercapacitors. Synthetic metals 2023; 298: 117447 https://doi.org/10.1016/j.synthmet.2023.117447

[14] Arora E.K., Sharma V., Ravi A., Shahi A., Jagtap S., Adhikari A., Dash J.K., Kumar P., Patel R. Polyaniline-Based Ink for Inkjet Printing for Supercapacitors, Sensors, and Electrochromic Devices. Energies 16(2023). https://doi.org/10.3390/en16186716

[15] J. Lin, Y. Yan, X. Zheng, Z. Zhong, Y. Wang, J. Qi, J. Cao, W. Fei, Y. Huang, J. Feng, Designing and constructing core-shell NiCo2S4@Ni3S2 on Ni foam by facile one-step strategy as advanced battery-type electrodes for supercapattery, Journal of Colloid and Interface Science 2019; 536: 456-462. https://doi.org/10.1016/j.jcis.2018.10.072

[16] M.S. Kumar, K.Y. Yasoda, S.K. Batabyal, N.K. Kothurkar, Carbon-polyaniline nanocomposites as supercapacitor materials, Materials Research Express 5 (2018). https://doi.org/10.1088/2053-1591/aab911

[17] T. Zheng, X.D. Wang, Y.Y. Liu, R. Bayaniahangar, H.B. Li, C.R. Lu, N. Xu, Z.D. Yao, Y.J. Qiao, D.X. Zhang, P. Abadi, Polyaniline-decorated hyaluronic acid-carbon nanotube hybrid microfiber as a flexible supercapacitor electrode material, Carbon 2020; 159: 65-73. https://doi.org/10.1016/j.carbon.2019.11.074

[18] Y. Zhu, C.W. Tan, S.L. Chua, Y.D. Lim, B. Vaisband, B.K. Tay, E.G. Friedman, C.S. Tan, Assembly Process and Electrical Properties of Top-Transferred Graphene on Carbon Nanotubes for Carbon-Based 3-D Interconnects, Ieee Transactions on Components Packaging and Manufacturing Technology 2020; 10: 516-524. https://doi.org/10.1109/TCPMT.2019.2940511

[19] Y. Cai, X. Li, X. Ren, L. Cheng, Y. Li, T. Liu, S. Huang, Preparation of carbon nanotubes/polyaniline buckypaper composite electrode by directional pressure filtration and its electrochemical properties, Acta Materiae Compositae Sinica 39 (2022) 664-676.

[20] T.Q. Hao, W. Wang, D. Yu, A Flexible Cotton-Based Supercapacitor Electrode with High Stability Prepared by Multiwalled CNTs/PANI, Journal of Electronic Materials 2018; 47: 4108-4115. https://doi.org/10.1007/s11664-018-6306-6

[21] Y. Cai, T. Liu, L. Cheng, S. Guo, S. Huang, Z. Hu, Y. Wang, H. Yu, D. Chen, Mechanical and electrochemical properties of carbon nanotubule-polyaniline nanowire/polyaniline nanoparticle high-strength ultra-flexible aerogel buckypaper, Colloids and Surfaces A: Physicochemical and Engineering Aspects 2024; 682: 132868. https://doi.org/10.1016/j.colsurfa.2023.132868

[22] P. Xie, W. Yuan, X.B. Liu, Y.M. Peng, Y.H. Yin, Y.S. Li, Z.P. Wu, Advanced carbon nanomaterials for state-of-the-art flexible supercapacitors, Energy Storage Materials 2021; 36: 56-76. https://doi.org/10.1016/j.ensm.2020.12.011

[23] T. Chen, L.M. Dai, Carbon nanomaterials for high-performance supercapacitors, Materials Today 2013; 16: 272-280. https://doi.org/10.1016/j.mattod.2013.07.002

[24] H.Y. Chen, S. Zeng, M.H. Chen, Y.Y. Zhang, Q.W. Li, Fabrication and functionalization of carbon nanotube films for high-performance flexible supercapacitors, Carbon 2015; 92: 271-296. https://doi.org/10.1016/j.carbon.2015.04.010

[25] Q. Jiang, Y. Shang, Y. Sun, Y. Yang, S. Hou, Y. Zhang, J. Xu, A. Cao, Flexible and multi-form solid-state supercapacitors based on polyaniline/graphene oxide/CNT composite films and fibers, Diamond and Related Materials 2019; 92: 198-207. https://doi.org/10.1016/j.diamond.2019.01.004

[26] X. Xiang, Z.J. Deng, H.F. Zhang, C.Q. Gao, S. Feng, Z.H. Liu, Q.Y. Liang, Y.F. Fu, Y.W. Liu, K. Liu, Polyaniline/polydopamine-regulated nitrogen-doped graphene aerogel with well-developed mesoporous structure for supercapacitor electrode, Chemical Engineering Journal 2023; 477: 147211. https://doi.org/10.1016/j.cej.2023.147211

[27] H.P. Xu, Q.L. Hu, T. Zhao, J.Q. Zhu; Z. Lian; X.J. Jin, Sodium carboxymethylcellulose/MXene/zeolite imidazolium framework-67-derived 3D porous carbon aerogel for high-performance asymmetric supercapacitors, Carbohydrate Polymers 2023; 326: 121642. https://doi.org/10.1016/j.carbpol.2023.121641

[28] Z.L. Chen, Y.L. Yang, T. Lv, Y.A. Liu, Y.L. Qi, K.Y. Dong, S.K. Cao, T. Chen, Designing free-standing 3D lamellar/pillared RGO/CNTs aerogels with ultra-high conductivity and compressive strength for elastic energy devices, Journal of Materials Chemistry A 2023; 11: 14187-14194. https://doi.org/10.1039/D3TA01531A

[29] T. Xu, Q. Song, K. Liu, H. Liu, J. Pan, W. Liu, L. Dai, M. Zhang, Y. Wang, C. Si, H. Du, K. Zhang, Nanocellulose-Assisted Construction of Multifunctional MXene-Based Aerogels with Engineering Biomimetic Texture for Pressure Sensor and Compressible Electrode, Nano-Micro Letters 15 (2023). https://doi.org/10.1007/s40820-023-01073-x

[30] S.K. Xu, S.R. Yan, X. Chen, H.F. Huang, X.Q. Liang, Y.H. Wang, Q. Hu, G.D. Wei, Y. Yang, Vertical porous Ti₃CNTx/rGO hybrid aerogels with enhanced capacitive performance, Chemical Engineering Journal 459 (2023). https://doi.org/10.1016/j.cej.2023.141528

[31] J. Ao, R. Miao, J.S. Li, Flexible solid-state supercapacitor based on reduced graphene oxide-enhanced electrode materials, Journal of Alloys and Compounds 2019; 802: 355-363. https://doi.org/10.1016/j.jallcom.2019.06.203

[32] Z.X. Hou, J.J. Li, C.Y. Qu, W. Li, K. Wang, 3D Double-Crosslinked Polyaniline/p-Phenylenediamine-Modified Graphene Free-Standing Electrodes for High-Performance Supercapacitors, Energy Technology 11 (2023). https://doi.org/10.1002/ente.202201447

[33] D.Y. Wu, J.J. Shao, Graphene-based flexible all-solid-state supercapacitors, Materials Chemistry Frontiers 2021; 5: 557-583. https://doi.org/10.1039/D0QM00291G

[34] J.F. Wu, Q.E. Zhang, J.J. Wang, X.P. Huang, H. Bai, A self-assembly route to porous polyaniline/reduced graphene oxide composite materials with molecular-level uniformity for high-performance supercapacitors, Energy & Environmental Science 2018; 11: 1280-1286. https://doi.org/10.1039/C8EE00078F

[35] M.G. Hosseini, E. Shahryari, Synthesis, Characterization and Electrochemical Study of Graphene Oxide-Multi Walled Carbon Nanotube-Manganese Oxide-Polyaniline Electrode as Supercapacitor, Journal of Materials Science & Technology 2016; 32: 763-773. https://doi.org/10.1016/j.jmst.2016.05.008

[36] Z.Q. He, D.D. Chen, M. Wang, C.X. Li, X.Y. Chen, Z.J. Zhang, Sulfur modification of carbon materials as well as the redox additive of Na₂S for largely improving capacitive performance of supercapacitors, Journal of Electroanalytical Chemistry 856 (2020). https://doi.org/10.1016/j.jelechem.2019.113678

[37] J.Q. Ye, Q. Shao, X.Y. Wang, T.R. Wang, Effects of B, N, P and B/N, B/P pair into zigzag single-walled carbon nanotubes: A first-principle study, Chemical Physics Letters 2016; 646: 95-101. https://doi.org/10.1016/j.cplett.2015.12.056

[38] C. Shao, C.K. Rui, J.X. Liu, A.Q. Chen, K.G. Zhu, Q.Y. Shao, First-Principles Study on the Electronic Transport Properties of B/P, B/As, and B/Sb Co-doped Single-Walled Carbon Nanotubes, Industrial & Engineering Chemistry Research 2020; 59: 19593-19599. https://doi.org/10.1021/acs.iecr.0c03804

[39] H. Fei, N. Saha, N. Kazantseva, T. Babkova, M. Machovsky, G. C. Wang, H. Bao, P. Saha, J. Mater. Polyaniline/reduced graphene oxide hydrogel film with attached graphite current collector for flexible supercapacitors Sci. Mater. Electron. 2018; 29: 3025. https://doi.org/10.1007/s10854-017-8233-3

[40] V. C. Tran, V. H. Nguyen, T. T. Nguyen, J. H. Lee, D. C. Huynh, J. J. Shim, Polyaniline and multi-walled carbon nanotube-intercalated graphene aerogel and its electrochemical properties. Synth. Met. 2016; 215: 150. https://doi.org/10.1016/j.synthmet.2016.02.017

[41] J.N. Ding, Peng Chen, Xuli Chen, and Kunkun Guo. Self-Assemble Strategy to Fabricate High Polyaniline Loading Nanocarbon Hydrogels for Flexible All-Solid-State Supercapacitors. ACS Appl. Energy Mater. 2021; 4: 3766-3776. https://doi.org/10.1021/acsaem.1c00176

[42] Wu, J.; Zhang, Q.; Wang, J.; Huang, X.; Bai, H. A self-assembly route to porous polyaniline/reduced graphene oxide composite materials with molecular-level uniformity for high-performance supercapacitors. Energy Environ. Sci. 2018; 11(5): 1280-1286. https://doi.org/10.1039/C8EE00078F

[43] Li, K.; Liu, J.; Huang, Y.; Bu, F.; Xu, Y. Integration of ultrathin graphene/polyaniline composite nanosheets with a robust 3D graphene framework for highly flexible all-solid-state supercapacitors with superior energy density and exceptional cycling stability. J. Mater. Chem. A 2017; 5(11): 5466-5474. https://doi.org/10.1039/C6TA11224B

[44] J. Chu, X. Li, Q. Li, J. Ma, B. Wu, X. Wang, R. Zhang, M. Gong, S. Xiong, Hydrothermal synthesis of PANI nanowires for high-performance supercapacitor. High Perform. Poly. 2019; 32: 258. https://doi.org/10.1177/0954008319856664

[45] Xing Zhang, Yanling Hao, and Wei Zhong, Boron-doped helical carbon nanotubes as active supercapacitor cathode materials: preparation and electrochemical properties. J Mater Sci: Mater Electron 2021; 32: 25269-25278. https://doi.org/10.1007/s10854-021-06984-2

[46] Lee, K., Cho, S., Heum Park, S. *et al*. Metallic transport in polyaniline. Nature 2006; 441: 65-68. https://doi.org/10.1038/nature04705

[47] Y. Yu, Y. Xi, J. Li, G. Wei, N. I. Klyui, W. Han, Flexible Supercapacitors Based on Polyaniline Arrays Coated Graphene Aerogel Electrodes. Nanoscale Res. Lett. 2017; 12: 394. https://doi.org/10.1186/s11671-017-2159-9

[48] R. F. Hu, J. Zhao, G. D. Zhu, J. P. Zheng, Fabrication of flexible free-standing reduced graphene oxide/polyaniline nanocomposite film for all-solid-state flexible supercapacitor. Electrochim. Acta 2018; 261: 151. https://doi.org/10.1016/j.electacta.2017.12.138

[49] C. M. Chang, Z. H. Hu, T. Y. Lee, Y. A. Huang, W. F. Ji, W. R. Liu, J. M. Yeh, Y. Wei, Biotemplated hierarchical polyaniline composite electrodes with high performance for flexible supercapacitors. J. Mater. Chem. A 2016; 4: 9133. https://doi.org/10.1039/C6TA01781A

[50] K. Jin, W. Zhang, Y. Wang, X. Guo, Z. Chen, L. Long, Z. Yao, Z. Wang, C. Jian, L. Sun, In-situ hybridization of polyaniline nanofibers on functionalized reduced graphene oxide films for high-performance supercapacitor. Electrochim. Acta 2018; 285: 221. https://doi.org/10.1016/j.electacta.2018.07.220

[51] NAWAZ S, KHAN Y, KHALID S, *et al*. Molybdenum disulfide (MoS2) along with graphene nanoplatelets (GNPs) utilized to enhance the capacitance of conducting polymers (PANI and PPy). RSC Advances, 2023; 13(41): https://doi.org/10.1039/D3RA04153K

[52] Xueyu Tao, Shifang Ye, Kehu Zhu, Liyang Dou, Peixin Cui, Jie Ma, Cheng Zhao, Xianyong Wei, Litong Guo, Akbar Hojjati-Najafabadi, and Peizhong Feng ACS Applied Energy Materials 2023; 6(15): 8177-8188. https://doi.org/10.1021/acsaem.3c01325

[53] Albdiry, M., Al-Nayili, A. Ternary sulfonated graphene/polyaniline/carbon nanotubes nanocomposites for high performance of supercapacitor electrodes. Polym. Bull. 2023; 80: 8245-8258. https://doi.org/10.1007/s00289-022-04495-6

[54] XU H, CUI L, PAN X, *et al*. Carboxymethylcellulose -polyaniline/carbon nanotube (CMC-PANI/CNT) film as flexible and highly electrochemical active electrode for supercapacitors. International Journal of Biological Macromolecules, 2022; 219: 1135-45. https://doi.org/10.1016/j.ijbiomac.2022.08.141

Received on 17-11-2023 Accepted on 20-12-2023 Published on 30-12-2023

DOI: https://doi.org/10.12974/2311-8717.2023.11.09